

## Determination of hyperfine splittings and Landé $g_J$ factors of $5s^2S_{1/2}$ and $5p^2P_{1/2,3/2}$ states of $^{111,113}\text{Cd}^+$ for microwave frequency standards

J. Z. Han<sup>1</sup>, R. Si<sup>2</sup>, H. R. Qin<sup>3</sup>, N. C. Xin<sup>1</sup>, Y. T. Chen<sup>1</sup>, S. N. Miao<sup>1</sup>, C. Y. Chen<sup>2,\*</sup>, J. W. Zhang<sup>1,†</sup> and L. J. Wang<sup>1,3,‡</sup>

<sup>1</sup>State Key Laboratory of Precision Measurement Technology and Instruments, Key Laboratory of Photon Measurement and Control Technology of Ministry of Education, Department of Precision Instrument, Tsinghua University, Beijing 100084, China

<sup>2</sup>Shanghai EBIT Lab, Key Laboratory of Nuclear Physics and Ion-Beam Application, Institute of Modern Physics, Department of Nuclear Science and Technology, Fudan University, Shanghai 200433, China

<sup>3</sup>Department of Physics, Tsinghua University, Beijing 100084, China



(Received 28 January 2022; revised 12 June 2022; accepted 14 July 2022; published 27 July 2022)

Regarding microwave frequency standards based on trapped ions, we report on the determination of the hyperfine splittings and the Landé  $g_J$  factors of  $^{111,113}\text{Cd}^+$ . The hyperfine splittings and Landé  $g_J$  factors of the  $5s^2S_{1/2}$  and  $5p^2P_{1/2,3/2}$  states of  $^{111,113}\text{Cd}^+$  are calculated using the multiconfiguration Dirac-Hartree-Fock scheme. Furthermore, the hyperfine splittings of the  $5p^2P_{3/2}$  state of  $^{111,113}\text{Cd}^+$  are derived based on the laser-induced fluorescence spectroscopy. The  $\text{Cd}^+$  ions are confined in a linear Paul trap and sympathetically cooled by laser-cooled  $\text{Ca}^+$  ions. The calculated values and the derived values are cross-checked, thereby guaranteeing the reliability of our results. The results provided in this paper can improve the signal-to-noise ratio of the clock transition and the accuracy of the second-order Zeeman shift correction, thus further improving the stability and accuracy of the microwave frequency standards based on trapped  $^{111,113}\text{Cd}^+$  ions.

DOI: [10.1103/PhysRevA.106.012821](https://doi.org/10.1103/PhysRevA.106.012821)

### I. INTRODUCTION

With the improvements in accuracy over time, atomic clocks have played an important role in both practical applications [1,2] and testing the fundamental physics [3–5]. Indeed, microwave clocks have played a vital role in satellite navigation [6], deep space exploration [7,8], and timekeeping [9]. Among many microwave clock proposals, those based on trapped ions have attracted wide attention from researchers because the ions are well isolated from the external environment in an ion trap. The setup is conducive to the improvements in the transportability of atomic clocks [10–13]. Microwave clocks based on trapped ions are also candidates for the next generation of practical atomic clocks [14].

Cadmium ions ( $^{111,113}\text{Cd}^+$ ) benefit from a simple and distinct electronic structure, which is easily controlled, manipulated, and measurable with high precision. The microwave frequency standard based on laser-cooled  $^{113}\text{Cd}^+$  ions has achieved an accuracy of  $1.8 \times 10^{-14}$  and a short-term stability of  $4.2 \times 10^{-13}/\sqrt{\tau}$  [15]. The high performance and potential for miniaturization make this frequency standard suitable for establishing a ground-based transportable frequency reference for navigation systems and for comparing atomic clocks between remote sites [15–18]. Moreover, it has been proposed as a means to achieve an ultrahigh level of accuracy down to  $10^{-15}$  [19], highlighting the importance of accurately evaluating their systematic frequency shifts.

Optical pumping is fundamental in operating a microwave frequency standard based on trapped ions. The optical pumping efficiency directly determines the signal-to-noise ratio of the “clock signal,” which affects the short-term stability and the measured accuracy of the ground-state hyperfine splitting (HFS) for such frequency standards. Realizing optical pumping for the  $^{111,113}\text{Cd}^+$  microwave frequency standard requires a blueshift in the laser frequency of the Doppler-cooling transition  $5s^2S_{1/2} (F = 1, m_F = 1) \rightarrow 5p^2P_{3/2} (F = 2, m_F = 2)$  to reach the  $5p^2P_{3/2} (F = 1)$  hyperfine level. Thus, the HFS of the  $5p^2P_{3/2}$  state is important for the optical pumping process. The HFSs for the ground and excited states of  $^{111,113}\text{Cd}^+$  were previously measured by the collinear laser spectroscopy in a fast ion-beam experiment [20]. However, for the HFSs of the  $5s^2S_{1/2}$  state of  $^{111,113}\text{Cd}^+$ , the results measured in a fast ion beam are larger than the results measured in an ion trap [15–18,21,22] and there is no overlap within their margins of uncertainty. A preliminary measurement of the HFS for the  $5p^2P_{3/2}$  state of  $^{111,113}\text{Cd}^+$  in the ion trap was approximately 800 MHz [21]. Therefore, a high-precision measurement for the HFSs of the  $5p^2P_{3/2}$  state of  $^{111,113}\text{Cd}^+$  in the ion trap would be an excellent addition and benchmark for the fast ion-beam experiment. A more reliable and accurate HFS of the  $5p^2P_{3/2}$  state of  $^{111,113}\text{Cd}^+$  will further improve the efficiency of the optical pumping and the performance of  $^{111,113}\text{Cd}^+$  microwave frequency standards. From the perspective of atomic structure calculations, high-precision measurements of the HFS can also be used for testing and developing the computation models in atomic structure calculations.

In a microwave frequency standard based on trapped ions, an external magnetic field is applied to provide the quantization axis to break the degeneracy of the ground-state magnetic

\*chychen@fudan.edu.cn

†zhangjw@tsinghua.edu.cn

‡lwang@mail.tsinghua.edu.cn

levels. Among all the systematic shifts of such frequency standard, the dominant one is the second-order Zeeman shift (SOZS) induced by the external magnetic field [15,23,24]. The precise estimation of the SOZS and the calibration of the external magnetic field require accurate knowledge of the ground-state Landé  $g_J$  factor [25]. There are only two theoretical studies that have provided a value of the ground-state Landé  $g_J$  factor in  $\text{Cd}^+$ : one giving 2.002 86(53), calculated using a relativistic-coupled-cluster (RCC) theory [25], and the other giving 2.002 291(4), calculated by a  $\Lambda$ -approach RCC ( $\Lambda$ -RCC) theory [26]. The two Landé  $g_J$  factors have a difference of 0.0006 that generates a fractional SOZS of  $6.6 \times 10^{-14}$  in an 0.08-G external magnetic field [15]. The large SOZS obviously reduces the accuracy of our latest  $^{113}\text{Cd}^+$  microwave frequency standard ( $1.8 \times 10^{-14}$ ) [15]. Therefore, redetermining the ground-state Landé  $g_J$  factor of  $^{113}\text{Cd}^+$  is imperative if the accuracy for this frequency standard is to be further improved.

In this paper, the HFSs and Landé  $g_J$  factors of the  $5s^2S_{1/2}$  and  $5p^2P_{1/2,3/2}$  levels are calculated using the multiconfiguration Dirac-Hartree-Fock (MCDHF) method. Electron correlation effects are carefully investigated and considered. The off-diagonal terms are included to improve the calculation accuracy of the HFSs for the  $5p^2P_{1/2,3/2}$  levels of  $^{111,113}\text{Cd}^+$ . Furthermore, the HFSs of the  $5p^2P_{3/2}$  state of  $^{111,113}\text{Cd}^+$  are derived based on the laser-induced fluorescence (LIF) technique. The  $^{111,113}\text{Cd}^+$  ions are sympathetically cooled to a low temperature by laser-cooled  $^{40}\text{Ca}^+$  ions, thus improving the accuracy of measurements. Cross-checking the calculated and measured HFSs ensures the reliability and accuracy of the results provided in this paper. The results reported in this paper are of great importance for further improving the performance of the microwave frequency standards based on trapped  $^{111,113}\text{Cd}^+$  ions.

## II. THEORY

### A. Multiconfiguration Dirac-Hartree-Fock approach

The MCDHF method [27], as implemented in the GRASP package [28,29], is employed to obtain wave functions referred to as atomic state functions. Specifically, they are approximate eigenfunctions of the Dirac Hamiltonian describing a Coulombic system given by

$$H_{\text{DC}} = \sum_{i=1}^N (c \boldsymbol{\alpha}_i \cdot \mathbf{p}_i + (\beta_i - 1)c^2 + V_i) + \sum_{i<j}^N \frac{1}{r_{ij}}, \quad (1)$$

where  $V_i$  denotes the monopole part of the electron-nucleus interaction for a finite nucleus and  $r_{ij}$  is the distance between electrons  $i$  and  $j$ ;  $\boldsymbol{\alpha}_i$  and  $\beta_i$  are the Dirac matrices for electron  $i$ .

Electron correlations are included by expanding  $|\Gamma J\rangle$ , an atomic state function, over a linear combination of configuration state functions (CSFs)  $|\gamma J\rangle$ :

$$|\Gamma J\rangle = \sum_{\gamma} c_{\gamma} |\gamma J\rangle, \quad (2)$$

where  $\gamma$  represents the parity and all the coupling tree quantum numbers needed to define the CSF uniquely. The CSFs are four-component spin-angular coupled, antisymmetric

products of Dirac orbitals of the form

$$\phi(\mathbf{r}) = \frac{1}{r} \begin{pmatrix} P_{n\kappa}(r) \chi_{\kappa m}(\theta, \phi) \\ i Q_{n\kappa}(r) \chi_{-\kappa m}(\theta, \phi) \end{pmatrix}. \quad (3)$$

The radial parts of the one-electron orbitals and the expansion coefficients  $c_{\gamma}$  of the CSFs are obtained by the self-consistent relativistic field procedure. In the following calculations of the relativistic configuration interaction (RCI), the Dirac orbitals are kept fixed, and only the expansion coefficients of the CSFs are determined for selected eigenvalues and eigenvectors of the complete interaction matrix. This procedure includes the Breit interaction and the leading quantum electrodynamic (QED) effects (vacuum polarization and self-energy).

The restricted active set method obtains the CSF expansions by allowing single and double (SD) substitutions from selected reference configurations to given orbitals to an active set (AS) of given orbitals [30]. The active set increases by increasing the number of layers, specifically, a set of virtual orbitals specified by its principal quantum number. We sort the electron correlation effects into three types: (i) substitutions only from the outermost valence subshells, where valence-valence correlation is included; (ii) at the most one substitution from the core subshell, where core-valence (CV) correlation is accounted for; and (iii) double substitutions from the core subshells, where core-core (CC) correlation is included. In this paper, the  $5s$  and  $5p$  subshells are defined as valence subshells, and the other inner subshells are core subshells.

The interaction between the electrons and the electromagnetic multipole moments of the nucleus splits each fine-structure level into multiple hyperfine levels. The interaction couples the nuclear spin  $\mathbf{I}$  with the total electronic angular momentum  $\mathbf{J}$  to obtain total angular momentum  $\mathbf{F} = \mathbf{I} + \mathbf{J}$ .

The hyperfine contribution to the Hamiltonian is represented by a multipole expansion:

$$H_{\text{HFS}} = \sum_{k \geq 1} \mathbf{T}^{(k)} \mathbf{M}^{(k)}, \quad (4)$$

where  $\mathbf{T}^{(k)}$  and  $\mathbf{M}^{(k)}$  are spherical tensor operators of rank  $k$  in the electronic and nuclear spaces [31]. The  $k = 1$  term represents the magnetic dipole interaction, and the  $k = 2$  term represents the electric quadrupole interaction. Higher-order terms are minor and can often be neglected.

For the ions considered in this paper ( $^{111,113}\text{Cd}^+$  with  $I = 1/2$ ), only the magnetic dipole hyperfine constant is nonzero and the quadrupole constant is equal to zero. To first order, the fine-structure level  $\gamma J$  is then split according to

$$\begin{aligned} & \langle \Gamma I J F M_F | \mathbf{T}^{(1)} \mathbf{M}^{(1)} | \Gamma I J F M_F \rangle \\ & = (-1)^{I+J+F} \begin{Bmatrix} I & J & F \\ J & I & 1 \end{Bmatrix} \langle \Gamma J || \mathbf{T}^{(1)} || \Gamma J \rangle \langle \Gamma I || \mathbf{M}^{(1)} || \Gamma I \rangle, \end{aligned} \quad (5)$$

where the coefficient in curly brackets is the  $6j$  symbol of the rotation group. The reduced matrix elements of the nuclear tensor operators are related to the conventional nuclear magnetic dipole moment:

$$\langle \Gamma I || \mathbf{M}^{(1)} || \Gamma I \rangle = \mu_N \sqrt{\frac{(2I+1)(I+1)}{I}}. \quad (6)$$

The hyperfine interaction energy contribution to a specified hyperfine level is then given by

$$\langle \Gamma I J F M_F | T^{(1)} M^{(1)} | \Gamma I J F M_F \rangle = \frac{1}{2} A_J C, \quad (7)$$

where  $A_J$  is the magnetic dipole hyperfine constant

$$A_J = \frac{\mu_I}{I} \frac{1}{\sqrt{J(J+1)}} \langle \gamma J || T^{(1)} || \gamma J \rangle, \quad (8)$$

and  $C = F(F+1) - J(J+1) - I(I+1)$ .

However, this method discards the off-diagonal hyperfine interaction, which is insufficient for  $^2P_{1/2,3/2}$  because the hyperfine interaction between the two  $F=1$  hyperfine levels is non-negligible owing to their minor splitting. To account for the off-diagonal hyperfine effects, we consider the second-order hyperfine interaction between  $^2P_{1/2,3/2}$ . The contribution associated with the sublevel labeled  $\gamma I J F M_F$  can be expressed as

$$\frac{|\langle \gamma I J F M_F | H_{\text{HFS}} | \gamma' I' J' F M_F \rangle|^2}{E_J - E_{J'}}. \quad (9)$$

In relativistic theory, choosing the direction of the magnetic field as the  $z$  direction and neglecting all diamagnetic contributions, the interaction between the magnetic moment of an atom in an external field  $B$  can be written as

$$H_M = (N_0^{(1)} + \Delta N_0^{(1)}) B, \quad (10)$$

where the first term is an operator of the same tensorial form as the magnetic dipole hyperfine operator, and the last term is the Schwinger QED correction due to QED corrected electronic  $g$ -factor value  $g_s = 2.00232$  [32]. The Landé  $g_J$  factor is expressed in terms of

$$g_J = \frac{\langle \Gamma J || N^{(1)} + \Delta N^{(1)} || \Gamma J \rangle}{\sqrt{J(J+1)}}. \quad (11)$$

In weak magnetic field, the interaction energy is small compared to the hyperfine-structure separation. In such condition, a hyperfine level is split according to

$$E_{Z_{\text{Zeeman}}} = g_F M_F \mu_B B, \quad (12)$$

where  $g_F$  is given by

$$g_F = \frac{F(F+1) + J(J+1) - I(I+1)}{2F(F+1)} g_J. \quad (13)$$

### B. Computation strategy

We start from the DHF calculation for the states of the  $4d^{10}5s$  and  $4d^{10}5p$  configurations, which use the extended optimal-level scheme [33]. The occupied orbitals are determined simultaneously and maintained throughout subsequent calculations. The strong pair correlations represented by substitutions of the form  $4d^2 \rightarrow 4f^2$  and  $4d^2 \rightarrow 5d^2$  do not allow us to include only the valence correlation of the single valence  $5s/5p$  electron. Hence, our first MCDHF (MCDHF1) calculation starts from the  $CC_{4d}$  mode, in which the  $5s/5p$  and  $4d$  electrons in the  $4d^{10}5s$  and  $4d^{10}5p$  reference configurations can be SD excited to  $n \leq 8, l \leq 6$  ( $AS_8$ , where “8” labels the maximum principal quantum number in the corresponding AS). To investigate the correlation effects of the inner core electrons, we perform a few RCI calculations using the one-electron radial functions derived from

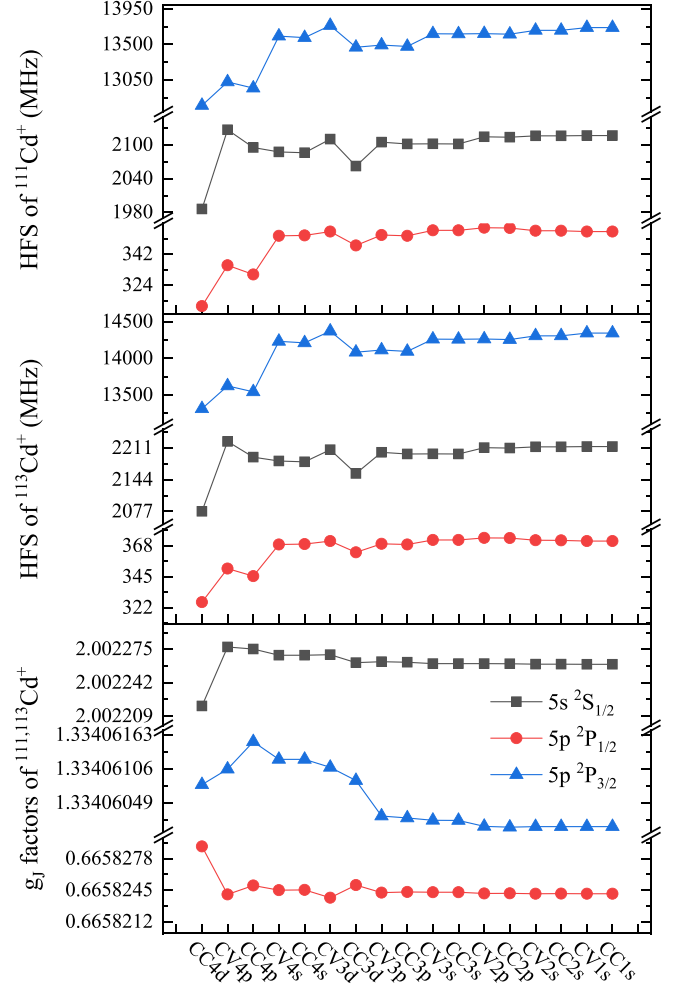


FIG. 1. Calculated hyperfine-structure constants  $A_J$  and Landé  $g_J$  factors of the  $4d^{10}5s^2S_{1/2}$  and  $4d^{10}5p^2P_{1/2,3/2}$  levels for  $^{111,113}\text{Cd}^+$ , from various correlation models used in the MCDHF1+RCI calculation.

the MCDHF1 procedure. We label the calculation method MCDHF1+RCI, where SD substitutions from inner core subshells down to  $1s$  are allowed step by step. As shown in Fig. 1, the  $A_J$  and  $g_J$  factors are sensitive to the core correlations, even to the  $1s$  subshell CV correlation. A second calculation (MCDHF2+RCI) is performed to describe better the wave functions that include the strong CV and CC correlations in the MCDHF procedure rather than only in the RCI procedure. In this calculation, the CV and CC correlations of the  $4d, 4p, 4s, 3d,$  and  $3p$  subshells and the CV correlation down to the  $1s$  subshell by allowing restricted SD excitations from the  $4d^{10}5s$  and  $4d^{10}5p$  reference configurations to  $n \leq 12, l \leq 6$  ( $AS_{12}$ ) are included. The RCI calculations are also performed to include the Breit and QED effects. Note that this calculation also starts from the DHF calculation for the  $4d^{10}5s$  and  $4d^{10}5p$  configurations.

In analyzing the wave-function compositions from the MCDHF2+RCI calculation, we notice strong correlations between  $4d^{10}5s, 4d^8 4f^2 5s,$  and  $4d^9 4f 5p$  configurations, and between  $4d^{10}5p, 4d^8 4f^2 5p,$  and  $4d^8 5p 5d^2$  configurations. Therefore, instead of starting from the DHF calculation where

TABLE I. Calculated hyperfine splittings (HFS, in MHz) and Landé  $g_J$  factors of the  $4d^{10}5s^2S_{1/2}$  state of  $^{111,113}\text{Cd}^+$ .  $\nu_{\text{HFS},s}$  is the HFS in the  $5s^2S_{1/2}$  state. Estimated uncertainties are given in parentheses.

	MCDHF2+RCI			MCDHF3+RCI		
	$\nu_{\text{HFS},s}^{111}$	$\nu_{\text{HFS},s}^{113}$	$g_J$	$\nu_{\text{HFS},s}^{111}$	$\nu_{\text{HFS},s}^{113}$	$g_J$
AS <sub>5</sub>	11841	12386	2.002243	12925	13521	2.002242
AS <sub>6</sub>	13421	14040	2.002245	14096	14746	2.002247
AS <sub>7</sub>	13671	14301	2.002254	14414	15079	2.002250
AS <sub>8</sub>	13879	14518	2.002260	14476	15143	2.002256
AS <sub>9</sub>	13884	14524	2.002262	14515	15184	2.002257
AS <sub>10</sub>	13925	14567	2.002263	14541	15211	2.002257
AS <sub>11</sub>	13919	14561	2.002263	14532	15202	2.002257
AS <sub>12</sub>	13921	14562	2.002262	14537	15207	2.002257
Final	13921(360)	14563(380)	2.002262(14)	14536(380)	15206(400)	2.002257(13)

only  $4d^{10}5s$  and  $4d^{10}5p$  are included in the CSF list, the  $4d$  and  $5s/5p$  electrons are allowed to be SD excited to  $\{5s, 5p, 5d, 4f\}$  to generate the CSF list as a starting point in our third calculation (labeled as MCDHF3+RCI). The spectroscopic orbitals and the  $5d$  and  $4f$  orbitals are optimized together, and the correlation effect between the essential CSFs is included in the beginning. The MCDHF3+RCI calculation includes the CV and CC correlations in the MCDHF2+RCI calculation. The final AS<sub>12</sub> expansions consist of 129 451 CSFs over the  $J = 1/2$  symmetry for even parity, and 134 682 and 381 872 CSFs distributed over the  $J = 1/2$  and  $3/2$  symmetries for odd parity. The calculation of AS<sub>12</sub> in MCDHF3+RCI spends 8 h, utilizing 16 processors on a cluster with 500G RAM.

The calculated HFS and  $g_J$  factors with increasing ASs from MCDHF2+RCI and MCDHF3+RCI calculations are listed in Tables I and II, respectively. We can see fluctuations in our calculated HFSs with increasing AS size, but the values from the last few ASs generally tend to some specific value. Therefore, we take the average of the last three values (AS<sub>10</sub>, AS<sub>11</sub>, and AS<sub>12</sub>), with the maximum difference between them taken as the uncertainty caused by the limited  $n$  of the expansions. The uncertainty caused by the limited  $l$  of the expansions is estimated by cutting off the highest  $l$  to 5. Since, in our calculation, we only include SD substitutions from the  $4d^{10}5s$  and  $4d^{10}5p$  configurations, we also try to investigate the uncertainty caused by high-order substitutions, especially for triple substitutions from them. Due to the vast number of CSFs if triple substitution is allowed, we include  $4d^8 4f^2 5s$  and  $4d^8 5s 5d^2$  as reference configurations for even parity, and  $4d^8 4f^2 5p$  and  $4d^8 5p 5d^2$  for odd parity, and allow single substitution from all the subshells from them. Thus, we have included some critical triple substitutions from  $4d^{10}5s$  and  $4d^{10}5p$ . The deviations to this tentative calculation are taken to estimate the missed triple substitution. Another uncertainty of our hyperfine calculation comes from the point-dipole approximation for the nuclear magnetic moment. The contribution from the finite distribution of the nuclear magnetic moment across the nucleus is known as the Bohr-Weisskopf (BW) effect [34]. It is currently tough to obtain this information for heavy systems, so we give a rough estimation from the previous publications [35,36]. The BW effects for the HFSs of  $^2S_{1/2}$  and  $^2P_{1/2,3/2}$  states are

roughly estimated to be around 2 and 1%, which makes most of our estimated uncertainties. By adding the above possible uncertainties together, we give the final uncertainty of our calculated HFSs in the parentheses in Tables I and II.

For the  $4d^{10}5s^2S_{1/2}$  state, as no other levels have strong hyperfine interactions, only the diagonal contributions are included in its HFS. Although the final splitting for  $^{113}\text{Cd}^+$  from the MCDHF2+RCI calculation [14 563(380) MHz] is much smaller than the experiment (15 200 MHz), the MCDHF3+RCI calculation [15 206(400) MHz] shows a significant improvement with the experiment. The HFSs for the  $^2P_{3/2}$  state of  $^{111,113}\text{Cd}^+$  from MCDHF2+RCI/MCDHF3+RCI calculations are 727(20)/760(20) and 789(21)/826(22) MHz, in which the off-diagonal contributions are not included. Those values increase to 793(21)/830(22) MHz when the off-diagonal hyperfine interactions between  $^2P_{1/2,3/2}$  are included. The interaction element from the MCDHF3+RCI calculations is  $1.75 \times 10^4$  MHz, and the fine-structure splitting from the atomic spectra database of the National Institute of Standards and Technology is  $7.44 \times 10^7$  MHz [37].

In pure  $LS$  coupling, the Landé  $g_J$  factor can be analytically evaluated by

$$g_J(LS) = 1 + (g_s - 1) \frac{J(J+1) + S(S+1) - L(L+1)}{2J(J+1)}. \quad (14)$$

The  $g_J(LS)$  values for  $^2S_{1/2}$  and  $^2P_{1/2,3/2}$  states of  $^{111,113}\text{Cd}^+$  are 2.0032, 0.6656, and 1.3344. The  $g_J$  values calculated by MCDHF3+RCI for the above states are 2.002 257(13), 0.665 817(5), and 1.334 056(6), respectively. Those values calculated by the MCDHF3+RCI approach are consistent with the analytical results in pure  $LS$  coupling and the deviations generally coming from term mixing and relativistic effects. The calculation uncertainties are estimated from the limited  $l$  and  $n$  values in the active set, the missed high-order substitutions, and the inactive orbitals.

### III. EXPERIMENT

The nuclear spin of  $^{111,113}\text{Cd}$  is 1/2, their  $5s^2S_{1/2} \rightarrow 5p^2P_{3/2}$  transition is split into three components, and only one

TABLE II. Calculated hyperfine splittings (HFS, in MHz) and Landé  $g_J$  factors of the  $4d^{10}5p^2P_{1/2,3/2}$  levels of  $^{111,113}\text{Cd}^+$ .  $\nu_{\text{HFS},p}$  is the HFS in the  $p$  state without off-diagonal contributions, whereas  $\nu_{\text{HFS},p}+\text{off-diag.}$  refers to the HFS in the  $p$  state with off-diagonal contributions. Estimated uncertainties are given in parentheses.

	MCDHF2+RCI			MCDHF3+RCI				
	$\nu_{\text{HFS},p}^{111}$	$\nu_{\text{HFS},p}^{113}$	$g_J$	$\nu_{\text{HFS},p}^{111}$	$\nu_{\text{HFS},p}^{113}$	$\nu_{\text{HFS},p}^{111}+\text{off-diag.}$	$\nu_{\text{HFS},p}^{113}+\text{off-diag.}$	$g_J$
$4d^{10}5p^2P_{1/2}$								
5	1816	1900	0.665833	2061	2156	2067	2150	0.665829
6	2099	2196	0.665825	2267	2371	2270	2368	0.665821
7	2054	2148	0.665825	2255	2359	2259	2355	0.665820
8	2142	2241	0.665820	2310	2416	2314	2413	0.665814
9	2123	2220	0.665822	2300	2406	2304	2403	0.665818
10	2146	2245	0.665821	2324	2432	2328	2428	0.665818
11	2144	2243	0.665820	2316	2422	2319	2419	0.665816
12	2145	2244	0.665820	2319	2425	2322	2422	0.665816
Final	2140(48)	2239(50)	0.665821(4)	2314(50)	2420(52)	2317(50)	2417(52)	0.665817(5)
$4d^{10}5p^2P_{3/2}$								
5	546	571	1.334062	644	674	650	680	1.334056
6	699	732	1.334057	787	824	791	827	1.334052
7	699	731	1.334060	768	803	772	807	1.334056
8	727	761	1.334060	794	830	797	834	1.334056
9	722	755	1.334062	786	822	789	826	1.334058
10	729	763	1.334060	789	828	793	832	1.334055
11	728	762	1.334059	789	824	792	828	1.334057
12	729	762	1.334060	789	825	793	829	1.334056
Final	727(20)	760(20)	1.334061(5)	789(21)	823(22)	792(21)	830(22)	1.334056(6)

component ( $F = 1 \rightarrow F = 2$ ) is a cycling transition that can be measured with high accuracy in the ion trap. Therefore, an indirect way is used to derive the HFSs of the  $5p^2P_{3/2}$  state of  $^{111,113}\text{Cd}^+$ . We first measure the frequency shifts from the  $5s^2S_{1/2} (F = 1) \rightarrow 5p^2P_{3/2} (F = 2)$  transition of  $^{111,113}\text{Cd}^+$  to the  $5s^2S_{1/2} \rightarrow 5p^2P_{3/2}$  transition in  $^{114}\text{Cd}^+$ . Briefly, for the experimental setup (shown in Fig. 2 and see Ref. [19] for details), we prepare crystals of two ion species consisting of

approximately  $2 \times 10^5 \text{Ca}^+$  and  $4 \times 10^5 \text{Cd}^+$  ions in a linear Paul trap. The  $\text{Ca}^+$  and  $\text{Cd}^+$  ions are produced by selected photoionization using laser beams of wavelength 423 nm ( $\text{Ca } 4s^2^1S_0 \rightarrow 4s4p^1P_1$ ), 374 nm ( $\text{Ca } 4s4p^1P_1 \rightarrow \text{continuum}$ ), and 228 nm ( $\text{Cd } 5s^2^1S_0 \rightarrow 5s5p^1P_1$ ). The  $\text{Ca}^+$  are used as coolant ions that are Doppler cooled using laser beams of wavelength 397 nm ( $\text{Ca}^+ 4s^2S_{1/2} \rightarrow 4p^2P_{1/2}$ ) and 866 nm ( $\text{Ca}^+ 3d^2D_{3/2} \rightarrow 4p^2P_{1/2}$ ). The  $\text{Cd}^+$  ions are sympathetically

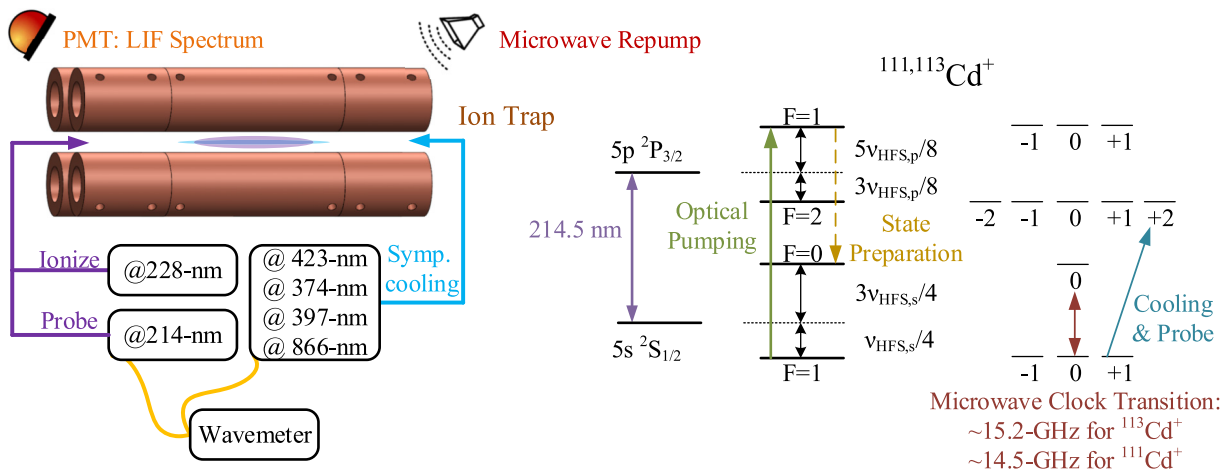


FIG. 2. Schematic of the experimental setup for deriving the HFSs of  $^{111,113}\text{Cd}^+$ . The sympathetic cooling technique is used to maintain the  $\text{Cd}^+$  ions at low temperatures and improve measurement accuracy. The energy-level scheme (not to scale) for  $^{111,113}\text{Cd}^+$  is also presented. PMT, photomultiplier tubes (Hamamatsu H8259-09).

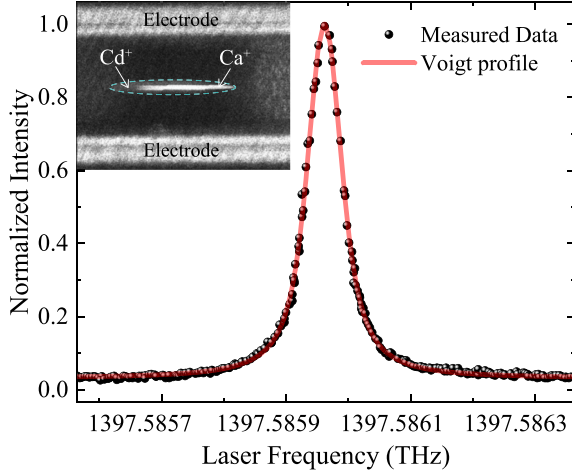


FIG. 3. Typical laser-induced fluorescence spectrum of  $\text{Cd}^+$ , using  $^{113}\text{Cd}^+$  as an example. The frequency of the probe laser beam (214.5 nm) is scanned around the resonance frequency over a range of 600 MHz. The measured line profile is fitted with a Voigt function. The inset is an image of the dual-species ion crystal of around  $10^5$   $\text{Cd}^+$  and  $\text{Ca}^+$  captured by an EMCCD camera. The aberration has blurred the image of  $\text{Cd}^+$  ions.

cooled to be around 100 mK through Coulomb interactions with the laser-cooled  $\text{Ca}^+$  ions. The frequency shifts of the  $5s^2S_{1/2} (F=1) \rightarrow 5p^2P_{3/2} (F=2)$  transition of  $^{111,113}\text{Cd}^+$  and the  $5s^2S_{1/2} \rightarrow 5p^2P_{3/2}$  transitions in  $^{114}\text{Cd}^+$  are measured by scanning the frequencies of a weak 214.5-nm probe laser beam. The  $5s^2S_{1/2} (F=1, m_F=1) \rightarrow 5p^2P_{3/2} (F=2, m_F=2)$  transition is a cycling transition that is used to probe the  $^{111,113}\text{Cd}^+$  ions. Although the circularly polarized probe laser beam excites a cycling transition, ions may, as a result of the polarization impurity, leak to the  $5s^2S_{1/2} (F=0)$  state via the  $5p^2P_{3/2} (F=1)$  state. A 23-dBm microwave radiation resonant with the ground-state hyperfine transition (15.2 GHz for  $^{113}\text{Cd}^+$  and 14.5 GHz for  $^{111}\text{Cd}^+$ ) is applied during LIF detection to increase detection efficiency. The frequency of each laser beam is measured using a high-precision wavemeter (HighFinesse WS8-2).

In obtaining the measured LIF spectrum (Fig. 3), the probe beam intensity is maintained below  $5 \mu\text{W}/\text{mm}^2$  (saturation intensity  $7.96 \text{ mW}/\text{mm}^2$  [38]) to reduce the cooling and heating effects of the probe laser beam. The fitted curve is the Voigt profile [19,39], expressed as

$$\begin{aligned}
 F(\nu) &= F_0 + [F_L(\nu) * F_G(\nu)], \\
 F_L(\nu) &= \frac{2A}{\pi} \frac{\nu_L}{4(\nu - \nu_c)^2 + \nu_L^2}, \\
 F_G(\nu) &= \sqrt{\frac{4 \ln 2}{\pi}} \frac{e^{-4 \ln 2 \nu^2 / \nu_G^2}}{\nu_G}, \quad (15)
 \end{aligned}$$

where  $F_0$  is the offset,  $\nu$  is the probe laser frequency,  $\nu_c$  is the ion resonance frequency,  $A$  is the area of the Lorentz profile,  $\nu_L$  is the Lorentzian width, and  $\nu_G$  is the Gaussian width of Doppler broadening. The line profile is slightly asymmetrical because of the heating and cooling effects of the probe beam, which lead to a slight increase in the uncertainty of the estimated transition frequency.

Measurements present three sources of uncertainty.

(i) *Statistical uncertainty.* For the  $5s^2S_{1/2} \rightarrow 5p^2P_{3/2}$  transition in  $\text{Cd}^+$ ,  $\nu_L$  is 60.13 MHz which represents the natural width, the fitted  $\nu_G$  is approximately 30 MHz, and the ion temperature is estimated to be approximately 0.1 K. The statistical uncertainty associated with the transition frequencies of  $^{114}\text{Cd}^+$  and  $^{111,113}\text{Cd}^+$  is approximately 1 MHz, and thus the statistical uncertainty in their differences is approximately 1.4 MHz.

(ii) *Instrumental uncertainty.* The uncertainty arising from the drift in the wavemeter is less than 0.5 MHz in our laboratory environment.

(iii) *Systematic shift uncertainty.* Most systematic shifts are common to the  $5s^2S_{1/2} \rightarrow 5p^2P_{3/2}$  transitions of both  $^{114}\text{Cd}^+$  and  $^{111/113}\text{Cd}^+$  and thus cancel each other out. The  $5s^2S_{1/2} (F=1) \rightarrow 5p^2P_{3/2} (F=2)$  transition of  $^{111/113}\text{Cd}^+$  is sensitive to magnetic fields; the Zeeman shift becomes the dominant contributor to systematic uncertainties. In a weak field ( $B \approx 0.08 \text{ G} \ll A/\mu_B$ ), the Zeeman shift for a specific energy level can be calculated by Eq. (12). By using values of  $g_J = 2.002257(13)$  and  $1.334056(6)$  for the states  $5s^2S_{1/2}$  and  $5p^2P_{3/2}$  calculated in this paper, the Zeeman shift for the  $5s^2S_{1/2} (F=1) \rightarrow 5p^2P_{3/2} (F=2)$  transition of  $^{111,113}\text{Cd}^+$  is estimated to be 0.11 MHz.

The final frequency differences  $\Delta \nu_{s,F=1 \rightarrow p,F=2}^{111/113,114}$  from the  $5s^2S_{1/2} (F=1) \rightarrow 5p^2P_{3/2} (F=2)$  of  $^{111/113}\text{Cd}^+$  to  $5s^2S_{1/2} \rightarrow 5p^2P_{3/2}$  of  $^{114}\text{Cd}^+$  are determined to be 4649.0(16)/4041.8(16) MHz. The numbers in parentheses are the estimated uncertainties, which are the square root of the sum of the square of the statistical uncertainties, instrumental uncertainties, and systematic shift uncertainties.

In *LS* coupling, the energy shift after the hyperfine interaction can be calculated by using Eq. (7). Therefore, for  $^{111,113}\text{Cd}^+$ , we have

$$\nu_{s,F=1 \rightarrow p,F=2}^{111/113} = \nu_{s \rightarrow p}^{111/113} + \frac{1}{4} \nu_{\text{HFS},s}^{111/113} - \frac{3}{8} \nu_{\text{HFS},p}^{111/113}, \quad (16)$$

where  $\nu_{s,F=1 \rightarrow p,F=2}^{111/113}$  is the frequency of the  $5s^2S_{1/2} (F=1) \rightarrow 5p^2P_{3/2} (F=2)$  transition in  $^{111/113}\text{Cd}^+$ ,  $\nu_{s \rightarrow p}^{111/113}$  represents the center of gravity of the optical transition  $5s^2S_{1/2} \rightarrow 5p^2P_{3/2}$  in  $^{111/113}\text{Cd}^+$ ,  $\nu_{\text{HFS},s}^{111/113}$  is the HFS of  $5s^2S_{1/2}$ , and  $\nu_{\text{HFS},p}^{111/113}$  is the HFS of  $5p^2P_{3/2}$  in  $^{111/113}\text{Cd}^+$ . In reference to  $^{114}\text{Cd}^+$ , through a linear transformation, Eq. (7) can be expressed as

$$\begin{aligned}
 \nu_{s,F=1 \rightarrow p,F=2}^{111/113} - \nu_{s \rightarrow p}^{114} &= \nu_{s \rightarrow p}^{111/113} - \nu_{s \rightarrow p}^{114} + \frac{1}{4} \nu_{\text{HFS},s}^{111/113} - \frac{3}{8} \nu_{\text{HFS},p}^{111/113}, \\
 \Delta \nu_{s,F=1 \rightarrow p,F=2}^{111/113,114} &= \Delta \nu_{s \rightarrow p}^{111/113,114} + \frac{1}{4} \nu_{\text{HFS},s}^{111/113} - \frac{3}{8} \nu_{\text{HFS},p}^{111/113}, \quad (17)
 \end{aligned}$$

where  $\Delta \nu_{s \rightarrow p}^{111/113,114}$  is 1314.3(22)[023]/555.2(23)[008] MHz measured in the fast ion-beam experiment of Ref. [40], and  $\nu_{\text{HFS},s}^{111/113}$  is 14 530.507 349 9(11)/15 199.862 854 96(12) MHz measured through the laser microwave double resonance spectroscopy of our previous work [16]. Therefore,  $\nu_{\text{HFS},p}^{111/113}$  is derived to be 794.6(36)/835.5(29) MHz. The uncertainty of  $\nu_{\text{HFS},p}^{111/113}$  mainly stems from the use of intermediate values of

TABLE III. Calculated HFSs and Landé  $g_J$  factors of  $5s^2S_{1/2}$  and  $5p^2P_{1/2,3/2}$  states, and the derived HFSs of the  $5p^2P_{3/2}$  state of  $^{111,113}\text{Cd}^+$ . Results of the HFSs and Landé  $g_J$  factors in  $\text{Cd}^+$  from other works are also listed for comparison. THU is the Tsinghua University in China, JPL is the Jet Propulsion Laboratory in USA, and CRL is the Communications Research Laboratory of Kansai Advanced Research Center in Japan.

$\nu_{\text{HFS}}^{111}$ (MHz)	$\nu_{\text{HFS}}^{113}$ (MHz)	$g_J$	Method	Type
		$5s^2S_{1/2}$		
14536(380)	15206(400)	2.002257(13)	MCDHF (This paper)	Theor.
14478(175)	15146(183)		RCC [41]	Theor.
	15280		RCC [42]	Theor.
		2.00286(53)	RCC [25]	Theor.
		2.002291(4)	$\Lambda$ -RCC [26]	Theor.
	15199.86285502799(27)		Ion trap (THU) [15]	Expt.
	15199.8628550287(10)		Ion trap (THU) [18]	Expt.
	15199.8628550125(87)		Ion trap (THU) [17]	Expt.
14530.5073499(11)	15199.86285496(12)		Ion trap (THU) [16]	Expt.
	15199.8628550(2)		Ion trap (JPL) [22]	Expt.
	15199.862858(2)		Ion trap (CRL) [21]	Expt.
14535.0(23)	15208.0(23)		Fast ion beam [20]	Expt.
		$5p^2P_{3/2}$		
792(21)	830(22)	1.334056(6)	MCDHF (This paper)	Theor.
794(12)	832(12)		RCC [41]	Theor.
	812.04		RCC [42]	Theor.
		1.33515(43)	RCC [25]	Theor.
794.6(36)	835.5(29)		Ion trap (THU) (This paper)	Expt.
	800		Ion trap (CRL) [21]	Expt.
796.4(10)	837.0(12)		Fast ion beam [20]	Expt.
		$5p^2P_{1/2}$		
2317(25)	2417(26)	0.665817(4)	MCDHF (This paper)	Theor.
2333(31)	2441(33)		RCC [41]	Theor.
	2430		RCC [42]	Theor.
		0.66747(83)	RCC [25]	Theor.

$\Delta\nu_{s \rightarrow p}^{111/113,114}$ . More precise values of  $\Delta\nu_{s \rightarrow p}^{111/113,114}$  will result in more precise  $\nu_{\text{HFS},p}^{111/113}$  values. The HFSs of the  $5p^2P_{3/2}$  state of  $^{111,113}\text{Cd}^+$  can be measured directly by using a deep ultraviolet electro-optic modulator with sidebands around 800 MHz, which will be conducted in future work.

#### IV. RESULTS AND DISCUSSIONS

The calculated HFSs and Landé  $g_J$  factors for the  $5s^2S_{1/2}$  and  $5p^2P_{1/2,3/2}$  states and the derived HFSs for the  $5p^2P_{3/2}$  states of  $^{111,113}\text{Cd}^+$  are listed in Table III; other experimental and theoretical results are also given for comparison. The present HFSs for the  $5s^2S_{1/2}$  state calculated using the MCDHF method show excellent agreement with previously measured results and those of the previous RCC results [41,42]. The central values of the MCDHF calculation are only around 6 MHz deviated from the central values of the ion trap experiment, while the RCC results are deviated by around 53 MHz. The agreement of the HFSs in the  $5s^2S_{1/2}$  state between the MCDHF calculation and the ion trap experiment further ensures the accuracy of our calculation of the Landé  $g_J$  factors in the  $5s^2S_{1/2}$  state. The high-accuracy measurements of HFSs for the  $5s^2S_{1/2}$  state of  $^{111,113}\text{Cd}^+$  in the ion trap provide an excellent benchmark for the atomic structure calculations and the fast ion-beam experiment.

However, the center values of the HFSs for the  $5s^2S_{1/2}$  state show some discrepancy between the fast ion-beam measurement [20] and the ion trap measurement [16,21,22], while the ion trap measurements from different groups showed consistency. The uncertainties given by the fast ion-beam experiments also do not cover the results of the ion trap experiments, suggesting that the uncertainty of the fast ion-beam experiments [20] may be underestimated.

The calculated HFSs for the  $5p^2P_{3/2}$  state also agree with the experiment and previous RCC results. The HFSs derived in this paper agree with those measured by the fast ion-beam experiment [20], and the central values are within each other's uncertainty range. The uncertainties of HFSs for the  $5p^2P_{3/2}$  state derived in this paper mainly stem from the use of intermediate values of the isotope shifts [40]. More precise values of the isotope shift will result in more accurate values of the HFSs in the  $5p^2P_{3/2}$  state. The derived HFSs for the  $5p^2P_{3/2}$  state in the ion trap experiment are slightly smaller than those of the fast ion-beam experiment, and this tendency also appeared in the HFSs for the  $5s^2S_{1/2}$  state. Therefore, the derived HFSs in this paper would be an excellent addition to the fast ion-beam experiment. The cross-checking between experiment and theory ensures the reliability of the HFSs for the  $5p^2P_{3/2}$  state of  $^{111,113}\text{Cd}^+$  determined in this paper. Thus, we recommend the values of 794.6(36)/835.5(29) MHz as the blueshifted frequencies for optical pumping in the microwave

frequency standard based on  $^{111/113}\text{Cd}^+$  ions. The frequency shifts from the  $5s^2S_{1/2} (F=1) \rightarrow 5p^2P_{3/2} (F=2)$  transition of  $^{111/113}\text{Cd}^+$  to the  $5s^2S_{1/2} \rightarrow 5p^2P_{3/2}$  transition of  $^{114}\text{Cd}^+$  measured in this paper would also be an excellent benchmark to the experiment of collinear laser spectroscopy on the fast ion-beam experiment, especially on the calibration of their acceleration voltages [43].

There are no experimental results regarding the Landé  $g_J$  factors in  $\text{Cd}^+$ . Accurate calculations of Landé  $g_J$  factors have proven to be complicated even for alkali-metal atoms and alkali-metal-like ions as they are sensitive to electron correlations. Those calculated in this paper using the MCDHF method show deviations from previous RCC results [2.00286(53)] [25]. The Landé  $g_J$  factor in the ground state calculated in this paper [2.002257(13)] agrees with the recent result calculated using the  $\Lambda$ -RCC theory [2.002291(4)] [26] to the fourth decimal place. However, there is no overlap within their margins of uncertainty. It is worth noticing that there also exists a deviation in the Landé  $g_J$  factor of  $^{171}\text{Yb}^+$  between the  $\Lambda$ -RCC theory [26] and the configuration interaction plus many-body perturbation theory [44]. Comparing the results of the same physical quantity from different calculation methods is also of great significance for developing atomic structure calculation models and investigating the role of electronic correlations. Therefore, we encourage more experimental and theoretical research on the Landé  $g_J$  factors of  $\text{Cd}^+$ .

In conservative estimation, we recommend 2.002 26(4) as the Landé  $g_J$  factor of the  $5s^2S_{1/2}$  state in  $\text{Cd}^+$  for evaluation of the SOZS of the microwave frequency standard based on trapped  $^{111,113}\text{Cd}^+$  ions. The SOZS of the  $5s^2S_{1/2} (F=0, m_F=0) \rightarrow 5s^2S_{1/2} (F=1, m_F=0)$  clock transition is given by [25]

$$\begin{aligned} \Delta\nu_{\text{SOZS}}(B) &= \frac{(g_J - g_I)^2 \mu_B^2 B^2}{2h^2 \nu_{\text{HFS},s}} \\ &= K_0 B^2, \end{aligned} \quad (18)$$

where  $\Delta\nu_{\text{SOZS}}(B)$  is the SOZS,  $K_0$  is the SOZS coefficient,  $g_J = 2.002\,26(4)$  is the recommended Landé  $g_J$  factor of the  $5s^2S_{1/2}$  state in  $\text{Cd}^+$ ,  $g_I = 0.622\,300\,9(9) \times 10^{-3}$  is the nuclear  $g$  factor in  $\text{Cd}^+$  [45],  $h$  is Planck's constant,  $\mu_B$  is the Bohr magneton, and  $\nu_{\text{HFS},s}$  is the HFS of the  $5s^2S_{1/2}$  state of  $^{111,113}\text{Cd}^+$ . The  $K_0$  is calculated to be 270.1(1) Hz/G<sup>2</sup> for  $^{111}\text{Cd}^+$  and 258.2(1) Hz/G<sup>2</sup> for  $^{113}\text{Cd}^+$ . Those values reported in this paper are consistent with the previous results [16,46,47] but with higher reliability. The uncertainty

of the SOZS coefficients stems from the Landé  $g_J$  factor which highlights the importance of a more accurate Landé  $g_J$  factor. For  $B \approx 0.08$  G, the external magnetic field for the  $\text{Cd}^+$  microwave frequency standard during actual operations [15], the fractional frequency shift is  $4.3 \times 10^{-15}$ . The shift produced by this Landé  $g_J$  factor can meet current accuracy requirements for the state-of-the-art  $\text{Cd}^+$  microwave frequency standard ( $1.8 \times 10^{-14}$  [15]). However, as the accuracy of the  $^{113}\text{Cd}^+$  microwave frequency standard is further improved to the order of  $10^{-15}$  [19], the precision of the Landé  $g_J$  factor should be at the sixth decimal to avoid an influence on the clock performance of such a frequency standard.

## V. CONCLUSION

We report on the determination of HFSs and Landé  $g_J$  factors for the  $5s^2S_{1/2}$  and  $5p^2P_{1/2,3/2}$  states of  $^{111,113}\text{Cd}^+$ . The HFSs and Landé  $g_J$  factors for all states of interest are calculated using the MCDHF method. Three computational strategies are followed to account for the electronic correlation effects comprehensively. Furthermore, we derive the HFSs of the  $5p^2P_{3/2}$  state for the  $^{111,113}\text{Cd}^+$  by combining our LIF data and previous measurements of isotope shifts and ground-state HFSs. The  $\text{Cd}^+$  ions are cotrapped with  $\text{Ca}^+$  ions in the same linear ion trap and sympathetically cooled through the Coulomb interaction with laser-cooled  $\text{Ca}^+$  ions. The calculated HFSs agree with the HFSs of this paper and our previous work, demonstrating the reliability of the theory and the experiment from cross-checks. The calculation and experiment conducted in this paper will be an excellent addition to the current atomic structure calculations [25,26,41,42] and the fast ion-beam experiments [20] in  $\text{Cd}^+$ . The HFSs and Landé  $g_J$  factors determined in this paper can improve the efficiency of the optical pumping procedure and the accuracy of the second-order Zeeman shift, which would further improve the stability and accuracy of the microwave frequency standard based on trapped  $^{111,113}\text{Cd}^+$  ions.

## ACKNOWLEDGMENTS

We thank W. X. Li, Z. M. Tang, and H. Wang for the helpful discussions. This work is supported by the National Key R&D Program of China (Grant No. 2021YFA1402100) and the National Natural Science Foundation of China (Grants No. 91436210, No. 12074081, and No. 12104095).

J.Z.H. and R.S. contributed equally to this work.

- 
- [1] N. Hinkley, J. A. Sherman, N. B. Phillips, M. Schioppo, N. D. Lemke, K. Beloy, M. Pizzocaro, C. W. Oates, and A. D. Ludlow, *Science* **341**, 1215 (2013).
  - [2] E. Burt, J. Prestage, R. Tjoelker, D. Enzer, D. Kuang, D. Murphy, D. Robison, J. Seubert, R. Wang, and T. Ely, *Nature (London)* **595**, 43 (2021).
  - [3] V. Dzuba, V. Flambaum, M. Safronova, S. Porsev, T. Pruttivarasin, M. Hohensee, and H. Häffner, *Nat. Phys.* **12**, 465 (2016).
  - [4] P. Wcisło, P. Morzyński, M. Bober, A. Cygan, D. Lisak, R. Ciuryło, and M. Zawada, *Nat. Astron.* **1**, 0009 (2017).
  - [5] M. S. Safronova, D. Budker, D. DeMille, D. F. J. Kimball, A. Derevianko, and C. W. Clark, *Rev. Mod. Phys.* **90**, 025008 (2018).
  - [6] T. Bandi, C. Affolderbach, C. E. Calosso, and G. Mileti, *Electron. Lett.* **47**, 698 (2011).
  - [7] J. D. Prestage and G. L. Weaver, *Proc. IEEE* **95**, 2235 (2007).

- [8] E. A. Burt, L. Yi, B. Tucker, R. Hamell, and R. L. Tjoelker, *IEEE Trans. Ultrason. Ferroelect. Freq. Contr.* **63**, 1013 (2016).
- [9] S. A. Diddams, J. C. Bergquist, S. R. Jefferts, and C. W. Oates, *Science* **306**, 1318 (2004).
- [10] P. D. Schwindt, Y.-Y. Jau, H. Partner, A. Casias, A. R. Wagner, M. Moorman, R. P. Manginell, J. R. Kellogg, and J. D. Prestage, *Rev. Sci. Instrum.* **87**, 053112 (2016).
- [11] S. Mulholland, H. Klein, G. Barwood, S. Donnellan, D. Gentle, G. Huang, G. Walsh, P. Baird, and P. Gill, *Appl. Phys. B* **125**, 198 (2019).
- [12] S. Mulholland, H. Klein, G. Barwood, S. Donnellan, P. Nisbet-Jones, G. Huang, G. Walsh, P. Baird, and P. Gill, *Rev. Sci. Instrum.* **90**, 033105 (2019).
- [13] T. M. Hoang, S. K. Chung, T. Le, J. D. Prestage, L. Yi, R. L. Tjoelker, S. Park, S.-J. Park, J. G. Eden, C. Holland *et al.*, *Appl. Phys. Lett.* **119**, 044001 (2021).
- [14] B. L. Schmittberger and D. R. Scherer, [arXiv:2004.09987](https://arxiv.org/abs/2004.09987).
- [15] S. Miao, J. Zhang, H. Qin, N. Xin, J. Han, and L. Wang, *Opt. Lett.* **46**, 5882 (2021).
- [16] J. W. Zhang, Z. B. Wang, S. G. Wang, K. Miao, B. Wang, and L. J. Wang, *Phys. Rev. A* **86**, 022523 (2012).
- [17] S. Wang, J. Zhang, K. Miao, Z. Wang, and L. Wang, *Opt. Express* **21**, 12434 (2013).
- [18] K. Miao, J. Zhang, X. Sun, S. Wang, A. Zhang, K. Liang, and L. Wang, *Opt. Lett.* **40**, 4249 (2015).
- [19] J. Han, H. Qin, N. Xin, Y. Yu, V. Dzuba, J. Zhang, and L. Wang, *Appl. Phys. Lett.* **118**, 101103 (2021).
- [20] D. T. Yordanov, D. L. Balabanski, J. Bieroń, M. L. Bissell, K. Blaum, I. Budinčević, S. Fritzsche, N. Frömmgen, G. Georgiev, C. Geppert, M. Hammen, M. Kowalska, K. Kreim, A. Krieger, R. Neugart, W. Nörtershäuser, J. Papuga, and S. Schmidt, *Phys. Rev. Lett.* **110**, 192501 (2013).
- [21] U. Tanaka, H. Imajo, K. Hayasaka, R. Ohmukai, M. Watanabe, and S. Urabe, *Phys. Rev. A* **53**, 3982 (1996).
- [22] B. M. Jelenković, S. Chung, J. D. Prestage, and L. Maleki, *Phys. Rev. A* **74**, 022505 (2006).
- [23] D. J. Berkeley, J. D. Miller, J. C. Bergquist, W. M. Itano, and D. J. Wineland, *Phys. Rev. Lett.* **80**, 2089 (1998).
- [24] P. Phoonthong, M. Mizuno, K. Kido, and N. Shiga, *Appl. Phys. B* **117**, 673 (2014).
- [25] J. Z. Han, Y. M. Yu, B. K. Sahoo, J. W. Zhang, and L. J. Wang, *Phys. Rev. A* **100**, 042508 (2019).
- [26] Y. M. Yu, B. K. Sahoo, and B. B. Suo, *Phys. Rev. A* **102**, 062824 (2020).
- [27] C. F. Fischer, M. Godefroid, T. Brage, P. Jönsson, and G. Gaigalas, *J. Phys. B* **49**, 182004 (2016).
- [28] P. Jönsson, G. Gaigalas, J. Bieroń, C. F. Fischer, and I. Grant, *Comput. Phys. Commun.* **184**, 2197 (2013).
- [29] C. F. Fischer, G. Gaigalas, P. Jönsson, and J. Bieroń, *Comput. Phys. Commun.* **237**, 184 (2019).
- [30] J. Olsen, B. O. Roos, P. Jørgensen, and H. J. A. Jensen, *J. Chem. Phys.* **89**, 2185 (1988).
- [31] E. W. McDaniel and M. R. C. McDowell, *Case Studies in Atomic Collision Physics* (Elsevier, Amsterdam, 2013).
- [32] K. T. Cheng and W. J. Childs, *Phys. Rev. A* **31**, 2775 (1985).
- [33] K. Dylla, I. Grant, C. Johnson, F. Parpia, and E. Plummer, *Comput. Phys. Commun.* **55**, 425 (1989).
- [34] A. Bohr and V. Weisskopf, *Phys. Rev.* **77**, 94 (1950).
- [35] F. Karpeshin and M. Trzhaskovskaya, *Nucl. Phys. A* **941**, 66 (2015).
- [36] B. M. Roberts, P. G. Ranclaud, and J. S. M. Ginges, *Phys. Rev. A* **105**, 052802 (2022).
- [37] A. Kramida, Y. Ralchenko, J. Reader, and NIST ASD Team, NIST Atomic Spectra Database (ver. 5.6.1) (National Institute of Standards and Technology, Gaithersburg, MD, 2018), <https://physics.nist.gov/asd>.
- [38] C. J. Foot, *Atomic Physics* (Oxford University, New York, 2004), Vol. 7.
- [39] Y. Zuo, J. Han, J. Zhang, and L. Wang, *Appl. Phys. Lett.* **115**, 061103 (2019).
- [40] M. Hammen, W. Nörtershäuser, D. L. Balabanski, M. L. Bissell, K. Blaum, I. Budinčević, B. Cheal, K. T. Flanagan, N. Frömmgen, G. Georgiev, C. Geppert, M. Kowalska, K. Kreim, A. Krieger, W. Nazarewicz, R. Neugart, G. Neyens, J. Papuga, P.-G. Reinhard, M. M. Rajabali, S. Schmidt, and D. T. Yordanov, *Phys. Rev. Lett.* **121**, 102501 (2018).
- [41] C.-B. Li, Y.-M. Yu, and B. K. Sahoo, *Phys. Rev. A* **97**, 022512 (2018).
- [42] G. Dixit, H. S. Nataraj, B. K. Sahoo, R. K. Chaudhuri, and S. Majumder, *Phys. Rev. A* **77**, 012718 (2008).
- [43] A. Kramida, *At. Data Nucl. Data Tables* **133**, 101322 (2020).
- [44] G. H. Gossel, V. A. Dzuba, and V. V. Flambaum, *Phys. Rev. A* **88**, 034501 (2013).
- [45] P. Spence and M. McDermott, *Phys. Lett. A* **42**, 273 (1972).
- [46] J. Vanier and C. Audoin, *The Quantum Physics of Atomic Frequency Standards* (Adam Hilger, Bristol, Philadelphia, 1989), Vol. 1.
- [47] U. Tanaka, H. Imajo, K. Hayasaka, R. Ohmukai, M. Watanabe, and S. Urabe, *IEEE Trans. Instrum. Meas.* **46**, 137 (1997).